Diffusion-driven destabilization of spatially homogeneous limit cycles in reaction-diffusion systems

Kuwamura, Masataka

Izuhara, Hirofumi

(Citation)
Chaos,27(3):033112-033112

(Issue Date)
2017-03

(Resource Type)
journal article

(Version)
Version of Record

Diffusion-driven destabilization of spatially homogeneous limit cycles in reaction-diffusion systems

Masataka Kuwamura and Hirofumi Izuhara

Citation: Chaos **27**, 033112 (2017); doi: 10.1063/1.4978924
View online: http://dx.doi.org/10.1063/1.4978924
View Table of Contents: http://aip.scitation.org/toc/cha/27/3
Published by the American Institute of Physics

Diffusion-driven destabilization of spatially homogeneous limit cycles in reaction-diffusion systems

Masataka Kuwamura[1,a)] and Hirofumi Izuhara[2,b)]
[1]Graduate School of Human Development and Environment, Kobe University, Kobe 657-8501, Japan
[2]Faculty of Engineering, University of Miyazaki, Miyazaki 889-2192, Japan

(Received 25 December 2016; accepted 6 March 2017; published online 24 March 2017)

We study the diffusion-driven destabilization of a spatially homogeneous limit cycle with large amplitude in a reaction-diffusion system on an interval of finite size under the periodic boundary condition. Numerical bifurcation analysis and simulations show that the spatially homogeneous limit cycle becomes unstable and changes to a stable spatially nonhomogeneous limit cycle for appropriate diffusion coefficients. This is analogous to the diffusion-driven destabilization (Turing instability) of a spatially homogeneous equilibrium. Our approach is based on a reaction-diffusion system with mass conservation and its perturbed system considered as an infinite dimensional slow-fast system (relaxation oscillator). *Published by AIP Publishing.*
[http://dx.doi.org/10.1063/1.4978924]

The diffusion-driven destabilization (Turing instability) is a fundamental principle for generating spatially nonhomogeneous patterns. In the same way as an equilibrium case, we consider the diffusion-driven destabilization of a spatially homogeneous limit cycle, which leads to a spatially nonhomogeneous limit cycle. We present a new method for constructing a spatially nonhomogeneous limit cycle with large amplitude in reaction-diffusion systems. In simple terms, our procedure is summarized as follows. First, we consider a 2-component ODE (ordinary differential equation) system in which the sum of the two components is conserved, i.e., $\dot{\mathbf{u}} = \mathbf{f}(\mathbf{u}, \mathbf{v})$ and $\dot{\mathbf{v}} = -\mathbf{f}(\mathbf{u}, \mathbf{v})$. Next, by adding perturbation terms, we construct a limit cycle of the perturbed ODE system by means of the theory of finite dimensional slow-fast systems, which are used for studying relaxation oscillations; two families of stable equilibria of the original ODE system are on this limit cycle. Third, by adding diffusion terms, we obtain a reaction-diffusion system considered as an infinite dimensional slow-fast system; the fast PDE (partial differential equation) system has a family of spatially unimodal stable equilibria induced by the diffusion-driven destabilization. Thus, to be discussed in detail later, from an analogy of the theory of finite dimensional slow-fast systems, we find that the reaction-diffusion system exhibits a spatially nonhomogeneous limit cycle with large amplitude, which is induced by the diffusion-driven destabilization. We explain these steps through a concrete example using numerical bifurcation analysis and simulations.

I. INTRODUCTION

Reaction-diffusion systems provide a theoretical framework for studying the mechanisms of biological pattern formation. In fact, they have been successfully applied to a wide range of developmental and ecological systems, see the textbooks.[23,24] This framework originates in a famous paper by Turing,[29] which shows that a spatially homogeneous equilibrium of a reaction-diffusion system becomes unstable for appropriate values of diffusion coefficients, although the equilibrium is stable in the corresponding ODE (ordinary differential equation) system without diffusion terms. This is called the diffusion-driven destabilization (Turing's instability) of an equilibrium. Many studies have been concerned with the diffusion-driven destabilization of a spatially homogeneous equilibrium because the mathematical analysis of this destabilization can be easily performed using the Fourier series expansion and transformation.

As in the case of equilibrium, we can consider that a spatially homogeneous limit cycle of a reaction-diffusion system becomes unstable for appropriate values of diffusion coefficients, although the limit cycle is stable in the corresponding ODE system without diffusion terms. In fact, Refs. 13 and 19 independently investigated the diffusion-driven destabilization of a spatially homogeneous limit cycle in a reaction-diffusion system defined on the whole real line. Although their methods are different from each other, their essential idea is explained as follows. Let $\phi(t)$ be a stable limit cycle of an ODE system. Then, we see that 1 is an eigenvalue (Floquet multiplier) of the monodromy matrix (Poincaré map) of the linearized ODE system around $\phi(t)$, and that its associated eigenvector is given by $\dot{\phi}(0) = \dot{\phi}(t)|_{t=0}$. Moreover, the absolute value of the other eigenvalues of this matrix is less than 1. For a reaction-diffusion system obtained from the ODE system by adding diffusion terms, we consider its linearization around $\phi(t)$ and apply the Fourier decomposition with respect to the spatial variable x. Then, we obtain a family of ODE systems with periodic coefficients, which is parameterized by the wavenumber k; each ODE system determines the growth of the amplitude of the corresponding Fourier mode. We note that 1 is an eigenvalue of the monodromy matrix of the ODE system corresponding to $k = 0$,

Note: Dedicated to the 75th birthday of Professor Masayasu Mimura.
a)e-mail: kuwamura@main.h.kobe-u.ac.jp
b)e-mail: izuhara@cc.miyazaki-u.ac.jp

because this system is the same as the linearization of the original ODE system around $\phi(t)$. Therefore, the monodromy matrix of an ODE system corresponding to a sufficiently small wavenumber can have an eigenvalue whose absolute value is greater than 1 for appropriate diffusion coefficients. This leads to a sufficient condition for the instability of a spatially homogeneous limit cycle in a reaction-diffusion system. For example, we can derive the Benjamin-Feir instability criterion of a spatially homogeneous limit cycle of the complex Ginzburg-Landau equation.[4,14] Their approach does not require any other conditions except that the spatial domain defined on reaction-diffusion systems is the whole real line.

The instability of a spatially homogeneous limit cycle indicated by the aforementioned approach of Refs. 13 and 19 is considered as a long wavelength instability, because the wavelength of a Fourier mode corresponding to a sufficiently small wavenumber is very long. In contrast, the instability determined by the growth of the amplitude of a Fourier mode corresponding to a general wavenumber can be captured under certain conditions. For example, the instability of a spatially homogeneous limit cycle with small amplitude near a Hopf bifurcation point can be investigated by asymptotic expansions (see Ref. 30 and the references therein). In particular, Ref. 26 showed the diffusion-driven destabilization of such a limit cycle near a Turing-Hopf bifurcation point in reaction-diffusion systems defined on a finite interval under the Neumann boundary condition.

The purpose of this paper is to investigate, from a different perspective, the diffusion-driven destabilization of a spatially homogeneous limit cycle with large amplitude in a simple reaction-diffusion model on a finite interval under the periodic boundary condition. The limit cycle is constructed by the theory of slow-fast ODE systems, which are used for studying relaxation oscillations.[1] The significant feature of slow-fast ODE systems is that their dynamics has two different time scales (see Fig. 4 in Section III). The van der Pol model for limit cycle behavior in the voltages and currents of electrical circuits, the FitzHugh-Nagumo model for periodic neuron firing of nerve action potential, and the Field-Noyes model for sustained periodic oscillations of cerium ions in Belousov-Zhabotinskii reaction are well-known examples of slow-fast ODE systems. See, for instance, the textbooks.[12,23,28] Our results show that the spatially homogeneous limit cycle becomes unstable and changes to a stable spatially nonhomogeneous limit cycle for appropriate diffusion coefficients. This is analogous to the diffusion-driven destabilization (Turing instability) of a spatially homogeneous equilibrium. It should be emphasized that the spatially nonhomogeneous limit cycle with large amplitude cannot be captured using the previous approaches.[13,19,26] Our approach is based on a reaction-diffusion system with mass conservation and its perturbed system considered as an infinite dimensional slow-fast system. We note that these systems originate from conceptual models for understanding cell polarization related to the directional movements of cell[10,20,25] and asymmetric cell division.[17,18] Although our approach is presented through a concrete example with the aid of numerical bifurcation analysis and simulations, our primary aim is to present a new method for constructing a spatially nonhomogeneous limit cycle with large amplitude, which is induced by the diffusion-driven destabilization.

The remainder of this paper is organized as follows. In Section II, we propose a simple slow-fast ODE model with a stable limit cycle. This model is obtained by a perturbation to an ODE system, where the sum of components is conserved. We present the essential idea of our approach through the finite dimensional ODE model. In Section III, we propose a two-component reaction-diffusion model by adding diffusion terms to the ODE model presented in Section II. This model is an infinite dimensional slow-fast system obtained by a perturbation to a reaction-diffusion system, where the total mass of the components is conserved. We demonstrate numerically that the spatially homogeneous limit cycle constructed by the ODE model in Section II becomes unstable and changes to a stable spatially nonhomogeneous limit cycle for appropriate diffusion coefficients. Here, we use a numerical scheme in Ref. 15 by adding a small white noise to prevent numerical solutions of our PDE (partial differential equation) system from dropping into the ODE dynamics. The effect of the white noise on numerical results is discussed in the Appendixes. Moreover, applying a numerical bifurcation analysis in Ref. 6, we explain the mechanism for generating such a spatially nonhomogeneous limit cycle in terms of the bifurcation structure of the unperturbed reaction-diffusion system. Concluding remarks are presented in Section IV.

II. CONSTRUCTION OF A SPATIALLY HOMOGENEOUS LIMIT CYCLE

Let us consider a slow-fast ODE system given by

$$\begin{cases} \dot{u} = f(u,v) + \varepsilon g(u,v) \\ \dot{v} = -f(u,v) + \varepsilon h(u,v), \end{cases} \tag{2.1}$$

where $\varepsilon > 0$ is sufficiently small, which implies that g and h are perturbation terms. By setting $\varepsilon = 0$, (2.1) is reduced to

$$\begin{cases} \dot{u} = f(u,v) \\ \dot{v} = -f(u,v), \end{cases} \tag{2.2}$$

which is the unperturbed system of (2.1). Notice that (2.2) satisfies the conservation property

$$u + v = s, \tag{2.3}$$

where s denotes a constant. It is easy to see that (2.2) gives the first stage of the dynamics of (2.1). In fact, a solution of (2.1) with an initial value $(\tilde{u}_0, \tilde{v}_0)$ moves along the line defined by $u + v = \tilde{u}_0 + \tilde{v}_0$ with a speed of $O(1)$, and approaches a family of stable equilibria of (2.2) given by

$$\Gamma = \{ (u,v) \,|\, f(u,v) = 0, f_u(u,v) < f_v(u,v) \}. \tag{2.4}$$

For example, when

$$f(u,v) = (uv - a)(u - b), \quad 0 < b < \sqrt{a} \tag{2.5}$$

we have $\Gamma = \Gamma_1 \cup \Gamma_2 \cup \Gamma_3$, where

$$\Gamma_1 = \{(u,v) | v = a/u, \ \sqrt{a} < u\}, \tag{2.6}$$

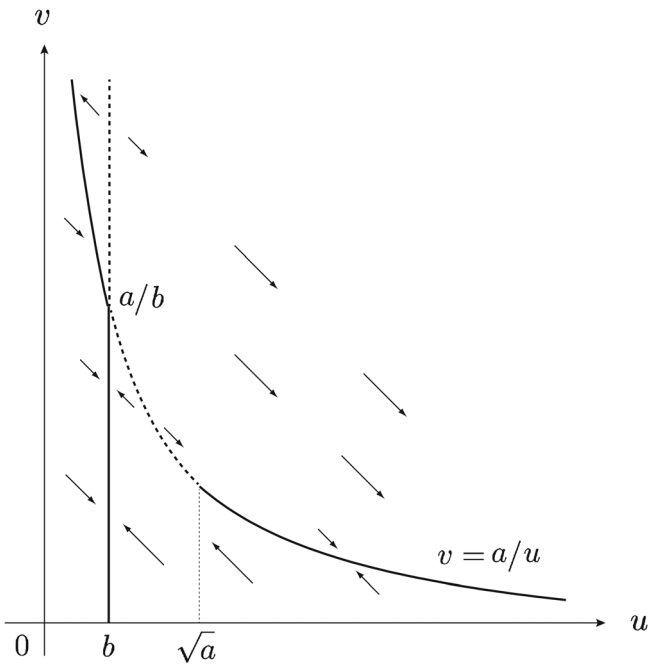

FIG. 1. The flow of (2.2) on the first quadrant of the uv-plane when $f(u, v)$ is given by (2.5). Here, the horizontal and vertical axes indicate u and v, respectively. The equilibria are given by $v = a/u$ or $u = b$. The solid line represents a family of stable equilibria Γ given by (2.4). On the other hand, the dashed line represents that of unstable equilibria.

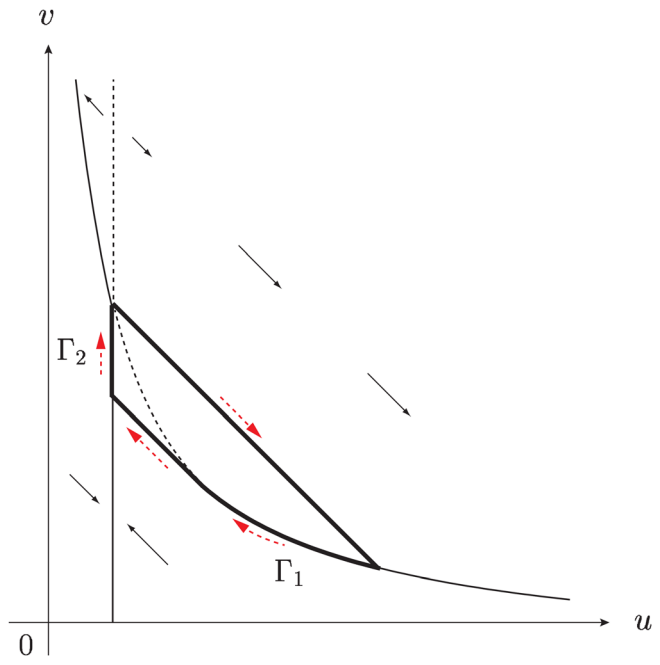

FIG. 2. A stable limit cycle of (2.1) on the first quadrant of the uv-plane when $f(u, v)$, $g(u, v)$, and $h(u, v)$ are given by (2.5) and (2.9), respectively. This is indicated by the bold closed curve, and the dashed arrows around the closed curve indicate the direction of the flow on the limit cycle. Γ_1 and Γ_2 are given by (2.6) and (2.7), respectively. Here, the horizontal and vertical axes indicate u and v, respectively.

$$\Gamma_2 = \{(u, v) | u = b,\ 0 < v < a/b\}, \tag{2.7}$$

and

$$\Gamma_3 = \{(u, v) | v = a/u,\ 0 < u < b\}. \tag{2.8}$$

This dynamics is called the fast dynamics of (2.1). For $f(u, v)$ given by (2.5), the flow of (2.2) on the first quadrant of the uv plane is shown in Fig. 1, which enables us to understand the fast dynamics of (2.1).

Once the solution of (2.1) reaches a neighborhood of the manifold Γ, it slowly moves along Γ following the dynamics defined by

$$\dot{s} = \varepsilon(g(u(s), v(s)) + h(u(s), v(s))),\ \ (u(s), v(s)) \in \Gamma,$$

where $s\,(= u(s) + v(s))$ gives a parametrization of Γ. This dynamics is called the slow dynamics of (2.1). For example, when

$$g(u, v) = \mu \ \text{ and } \ h(u, v) = -\rho(u - b)^2 \tag{2.9}$$

with

$$\mu < \rho(\sqrt{a} - b)^2, \tag{2.10}$$

we have

$$\dot{s} = \varepsilon(\mu - \rho(u - b)^2) < 0 \quad \text{on} \quad \Gamma_1 \tag{2.11}$$

and

$$\dot{s} = \varepsilon\mu > 0 \ \text{ on } \Gamma_2, \tag{2.12}$$

where Γ_1 and Γ_2 are manifolds defined by (2.6) and (2.7), respectively. When $f(u, v)$, $g(u, v)$, and $h(u, v)$ are given by (2.5) and (2.9), we see that (2.1) admits a stable limit cycle shown in Fig. 2.

We can also capture this limit cycle using the bifurcation structure of (2.2). Noting the conservation property (2.3), we rewrite (2.2) as

$$\dot{u} = f(u, s - u), \tag{2.13}$$

where s is a bifurcation parameter. Then, we can obtain the bifurcation diagram of (2.13) with respect to s, as presented

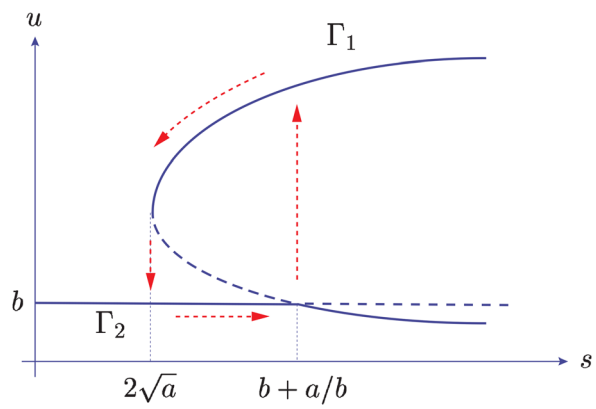

FIG. 3. The bifurcation diagram of (2.2) (equivalent to (2.13)) with respect to s when $f(u, v)$ is given by (2.5). Here, the horizontal and vertical axes indicate s and u, respectively. The solid line indicates stable solutions, whereas the dashed line indicates unstable ones. The dashed arrows indicate the dynamics of (2.1) when $f(u, v)$, $g(u, v)$, and $h(u, v)$ are given by (2.5) and (2.9), respectively. Those in the vertical direction indicate the fast dynamics given by (2.2), which drives the jump from Γ_1 (resp. Γ_2) to Γ_2 (resp. Γ_1). The other dashed arrows around Γ_1 and Γ_2 indicate the slow dynamics given by (2.11) and (2.12), respectively, where Γ_1 and Γ_2 are given by (2.6) and (2.7), respectively.

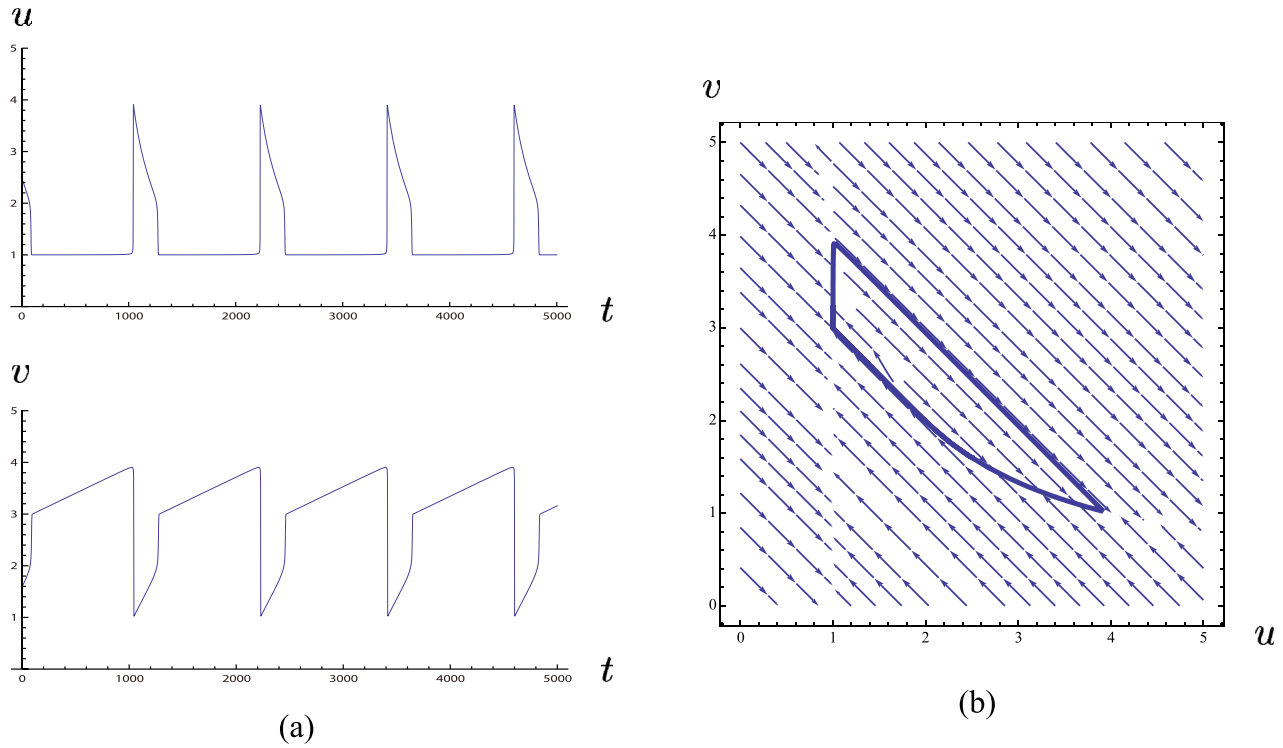

FIG. 4. The stable limit cycle of (2.1) with (2.5) and (2.9) for $\varepsilon = 0.01$ when $a = 4.0$, $b = 1.0$, $\mu = 0.1$, and $\rho = 0.15$. This limit cycle is a relaxation oscillation with two different time scales. (a) Time evolution of u and v. The values of u and v rapidly change in the fast dynamics, whereas these values slowly change in the slow dynamics. (b) The trajectory of the stable limit cycle on the first quadrant of the uv-plane.

in Fig. 3, which suggests the existence of the stable limit cycle of (2.1). As seen in Sec. III, an essential idea is that a conserved quantity of an unperturbed differential equation can be regarded as a bifurcation parameter. Once we have obtained the bifurcation diagram of the unperturbed equation, such as in Fig. 3, we investigate the dynamics of solutions moving along stable branches in the bifurcation diagram, which is driven by perturbation terms.

Finally, we demonstrate the stable limit cycle indicated by Figs. 2 and 3 numerically. By setting the values of the parameters as

$$a = 4.0,\ b = 1.0,\ \mu = 0.1,\ \rho = 0.15, \tag{2.14}$$

and $\varepsilon = 0.01$, we obtain the stable limit cycle shown in Fig. 4 by using Mathematica (ver. 9).

III. DESTABILIZATION OF A SPATIALLY HOMOGENEOUS LIMIT CYCLE

In this section, we consider a two-component reaction-diffusion system that is obtained by adding diffusion terms to (2.1), i.e.,

$$\begin{cases} \dot{u} = D_u u_{xx} + f(u,v) + \varepsilon g(u,v) \\ \dot{v} = D_v v_{xx} - f(u,v) + \varepsilon h(u,v) \end{cases} \quad (0 \le x \le 2\pi) \tag{3.1}$$

under the periodic boundary condition. We suppose that the diffusion coefficients D_u and D_v are positive constants satisfying

$$D_v \ge D_u. \tag{3.2}$$

Hereafter, following the previous section, our numerical bifurcation analysis, simulations, and calculations are performed by using the concrete expressions of $f(u, v)$, $g(u, v)$, and $h(u, v)$, which are given by (2.5) and (2.9).

The limit cycle presented in Sec. II is a spatially homogeneous limit cycle of (3.1). We investigate the diffusion-driven destabilization of the spatially homogeneous limit cycle of (3.1) which can be regarded as an infinite dimensional slow-fast system. Moreover, we are concerned with nonnegative solutions of (3.1). Furthermore, we use the parameter values given by (2.14) in our numerical simulations and bifurcation analysis. The same results can also be obtained near the specific parameter values given by (2.14).

A. Fast dynamics

We consider the fast dynamics of (3.1) given by

$$\begin{cases} \dot{u} = D_u u_{xx} + f(u,v) \\ \dot{v} = D_v v_{xx} - f(u,v), \end{cases} \tag{3.3}$$

which is obtained from (3.1) by setting $\varepsilon = 0$. This unperturbed system is called a reaction-diffusion system with mass conservation because

$$\int_0^{2\pi} (u(x,t) + v(x,t))dx \equiv \int_0^{2\pi} (u(x,0) + v(x,0))dx \tag{3.4}$$

holds for any (smooth) solutions. Such systems were originally proposed in Refs. 10 and 25 for understanding cell polarization related to the directional movements of cell.

First, we consider the (in)stability of spatially homogeneous equilibria of (3.3), which are stable in (2.2), the corresponding ODE system without the diffusion terms. Let $(u^*, v^*) \in \Gamma$ defined by (2.4). By applying a standard linear stability analysis, it is easy to see that (u^*, v^*) is stable if

$$D_v f_u^* - D_u f_v^* < 0,$$

where $f_u^* := f_u(u^*, v^*)$ and $f_v^* := f_v(u^*, v^*)$ satisfy $f_u^* < f_v^*$. On the other hand, (u^*, v^*) is unstable if

$$D_v f_u^* - D_u f_v^* > 0,$$

and the wavenumber of the unstable Fourier mode e^{ikx} satisfies

$$0 < k^2 < \frac{D_v f_u^* - D_u f_v^*}{D_u D_v}, \tag{3.5}$$

where $k \in \mathbf{N}$. When $f(u, v)$, $g(u, v)$, and $h(u, v)$ are given by (2.5) and (2.9), noting (2.10) and (3.2), we see that Γ_1^s, Γ_2, and Γ_3 are families of stable equilibria, where Γ_2 and Γ_3 are defined by (2.7) and (2.8), respectively, and

$$\Gamma_1^s = \{(u, v) | \, v = a/u, \ \sqrt{D_v a/D_u} < u\} \subset \Gamma_1$$

by virtue of (3.2). On the other hand, an equilibrium on Γ_1^u can be unstable, where

$$\Gamma_1^u = \{(u, v) | \, v = a/u, \ \sqrt{a} < u < \sqrt{D_v a/D_u}\} \subset \Gamma_1.$$

We note that Γ_1^s and Γ_1^u are manifolds parameterized by $s(=u+v)$, i.e.,

$$\Gamma_1^s = \{(u(s), v(s)) | \, s > s^*\}$$

and

$$\Gamma_1^u = \{(u(s), v(s)) | \, 2\sqrt{a} < s < s^*\},$$

where $s^* = \sqrt{aD_v/D_u} + \sqrt{aD_u/D_v}$. Moreover, we note that $\Gamma_1^u = \varnothing$ if $D_v = D_u$, which suggests that the spatially homogeneous limit cycle of (3.1) in Sec. II is stable if $D_v = D_u$.

From the above stability analysis, we expect that (3.3) has a family of spatially nonhomogeneous stable equilibria for $D_v > D_u$. In fact, our numerical simulations show that solutions with initial values near Γ_1^u eventually converge to a simple unimodal pattern (spike) for $D_v > D_u$ (Fig. 5). Noting the conservation property (3.4), we see that (3.3) has a family of unimodal stable equilibria Γ_4 parameterized by

$$s = \frac{1}{2\pi} \int_0^{2\pi} (u(x) + v(x)) dx \tag{3.6}$$

for $D_v > D_u$.

Remark 1. Concerning the dynamics of reaction-diffusion systems with mass conservation in Refs. 10 and 25, solutions with initial values near Γ_1^u eventually approach a single spike, as presented in Fig. 5, after exhibiting long transient dynamics. Here, spatial patterns consisting of spikes appear and the number of spikes decreases. The number of spikes appearing at the first stage of the dynamics mainly depends on the value of D_u. We choose $D_u = 0.2$ such that the number is equal to one. On the other hand, the amplitude of these mainly depends on D_v/D_u.

Remark 2. For appropriate functions f such as $f(u, v) = v - u/(u^2 + c)$ with $c > 0$, it was proved in Refs. 11, 21, and 22 that every stable equilibrium of (3.3) must be constant or unimodal under the periodic boundary condition.

Next, we demonstrate numerically that the bifurcation diagram of (3.3) contains a structure which generates a spatially nonhomogeneous limit cycle of (3.1). Let $w = u + v$. Then, (3.3) can be rewritten as

$$\begin{cases} \dot{w} = D_v w_{xx} + (D_u - D_v) u_{xx} \\ \dot{u} = D_u u_{xx} + f(u, w - u). \end{cases} \tag{3.7}$$

By using AUTO,[5] a software package used for studying the bifurcation structure of ODE systems, we investigate the bifurcation structure of an ODE system that is obtained by the finite Fourier series approximation for (3.7).

It should be noted that the linearized operator of (3.7) around any equilibrium has zero eigenvalue owing to its translation invariance for solutions under the periodic boundary condition. This fact implies that AUTO cannot trace branches of bifurcating solutions of an approximate ODE system for (3.7). Indeed, the Newton method for numerically capturing equilibria cannot converge because the linearized operator of the approximate ODE system around an equilibrium has (almost) zero eigenvalue. Therefore, we consider (3.7) under the boundary condition

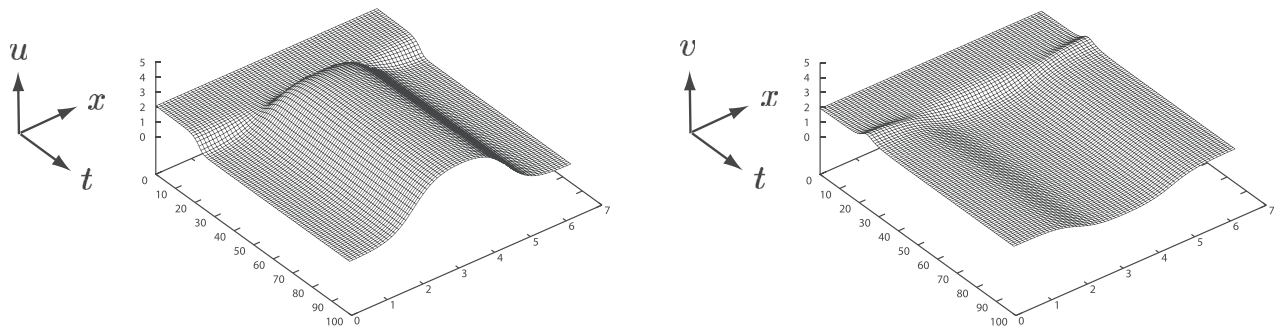

FIG. 5. The dynamics of the solution of (3.3) with an initial value near Γ_1^u when $f(u, v)$ is given by (2.5). The values of $u(x, t)$ (on the left) and $v(x, t)$ (on the right) for $0 \le x \le 2\pi$ and $0 \le t \le 100$ are represented by a 3D graph. Here, we translate these graphs in the x-direction in such a way the position of the peak of u is identical to $x = \pi$. In this numerical simulation, the values of the parameters are given by $a = 4.0$ and $b = 1.0$, and those of the diffusion coefficients are given by $D_u = 0.2$ and $D_v = 0.6$. Moreover, the initial value is given by $(2.1 + \varepsilon_1(x), \ 1.9 + \varepsilon_2(x))$, where $\varepsilon_1(x)$ and $\varepsilon_2(x)$ are independent uniform pseudorandom numbers in $[-0.005, 0.005)$ for each $x \in [0, 2\pi]$.

$$\begin{cases} w(0,t) = w(2\pi,t), \\ w_x(0,t) = w_x(2\pi,t) = 0, \\ u(0,t) = u(2\pi,t), \\ u_x(0,t) = u_x(2\pi,t) = 0, \end{cases} \tag{3.8}$$

which does not satisfy the translation invariance for solutions. We seek approximate solutions for (3.7) with (3.8) as

$$\begin{pmatrix} w(x,t) \\ u(x,t) \end{pmatrix} = \sum_{n=0}^{N} \begin{pmatrix} w_n(t) \\ u_n(t) \end{pmatrix} \cos nx. \tag{3.9}$$

Substituting (3.9) into (3.7) and comparing the coefficients of $\cos nx$ for each n, we obtain an ODE system for w_0, u_0, w_1, u_1, …, w_N, and u_N. For example, when $f(u, v)$ is given by (2.5) and $N = 2$, we have

$$\begin{cases} \dot{w}_0 = 0, \\ \dot{w}_1 = -D_v w_1 - (D_u - D_v)u_1, \\ \dot{w}_2 = -4D_v w_2 - 4(D_u - D_v)u_2, \\ \dot{u}_0 = \left(u_0^2 + \frac{1}{2}u_1^2 + \frac{1}{2}u_2^2\right)w_0 + \frac{1}{2}(2u_0u_1 + u_1u_2)w_1 + \frac{1}{2}\left(2u_0u_2 + \frac{1}{2}u_1^2\right)w_2 \\ \qquad -\left(u_0^3 + \frac{3}{2}u_0u_1^2 + \frac{3}{2}u_0u_2^2 + \frac{3}{4}u_1^2u_2\right) - au_0 - b\left(u_0w_0 + \frac{1}{2}u_1w_1 + \frac{1}{2}u_2w_2\right) \\ \qquad +b\left(u_0^2 + \frac{1}{2}u_1^2 + \frac{1}{2}u_2^2\right) + ab, \\ \dot{u}_1 = -D_u u_1 + (2u_0u_1 + u_1u_2)w_0 + \left(u_0^2 + \frac{1}{2}u_1^2 + \frac{1}{2}u_2^2\right)w_1 + \frac{1}{2}\left(2u_0u_2 + \frac{1}{2}u_1^2\right)w_1 \\ \qquad +\frac{1}{2}(2u_0u_1 + u_1u_2)w_2 + \frac{1}{2}u_1u_2w_2 - \left(3u_0^2u_1 + 3u_0u_1u_2 + \frac{3}{2}u_1u_2^2 + \frac{3}{4}u_1^3\right) \\ \qquad -au_1 - b\left(u_1w_0 + u_0w_1 + \frac{1}{2}u_2w_1 + \frac{1}{2}u_1w_2\right) + b(2u_0u_1 + u_1u_2), \\ \dot{u}_2 = -4D_u u_2 + \left(2u_0u_2 + \frac{1}{2}u_1^2\right)w_0 + \frac{1}{2}(2u_0u_1 + u_1u_2)w_1 + \frac{1}{2}u_1u_2w_1 \\ \qquad +\left(u_0^2 + \frac{1}{2}u_1^2 + \frac{1}{2}u_2^2\right)w_2 + \frac{1}{4}u_2^2w_2 - \left(3u_0^2u_2 + \frac{3}{2}u_0u_1^2 + \frac{3}{2}u_1^2u_2 + \frac{3}{4}u_2^3\right) \\ \qquad -au_2 - b\left(u_2w_0 + \frac{1}{2}u_1w_1 + u_0w_2\right) + b\left(\frac{1}{2}u_1^2 + 2u_0u_2\right). \end{cases}$$

Notice that the above system is the suspension of an ODE system for w_1, w_2, u_0, u_1, and u_2 with a bifurcation parameter w_0. Moreover, we note that w_0 corresponds to the conserved quantity of (3.3) defined by (3.6). Therefore, for large N, the ODE system for $w_1, \ldots, w_N$, $u_0, u_1, \ldots, u_N$ given by

$$\begin{cases} \dot{w}_1 = -D_v w_1 - (D_u - D_v)u_1 \\ \qquad \vdots \\ \dot{w}_N = -D_v N^2 w_N - (D_u - D_v)N^2 u_N \\ \dot{u}_0 = u_0^2 s + \frac{1}{2}u_1^2 s + \cdots \\ \dot{u}_1 = -D_u u_1 + 2u_0u_1 s + u_1u_2 s + \cdots \\ \qquad \vdots \\ \dot{u}_N = -D_u N^2 u_N + 2u_0u_N s + u_0^2 w_N + \cdots \end{cases} \tag{3.10}$$

can provide an approximation for (3.7) with (3.8), where s is a bifurcation parameter corresponding to the conserved quantity of (3.3) defined by (3.6).

We investigate the bifurcation structure of (3.10) with $N = 30$. We choose $N = 30$ with a margin for numerical errors although we confirm that the bifurcation structure of (3.10) does not depend on N for $N > 20$.

Fig. 6(a) shows that the bifurcation diagram of (3.10) with respect to s for $D_u = D_v = 0.2$ contains the same structure as in that of (2.2), which is presented in Fig. 3. Moreover, notice that the set consisting of bifurcating branches of stable solutions in Fig. 6(a) is included in the bifurcation diagram of (3.10) with respect to s for $D_u = 0.2$ and $D_v = 0.6$, as presented in Fig. 6(b). Fig. 7 provides a magnification of the rectangular region $[4.3, 4.8] \times [7.5, 9.5]$ in Fig. 6(b). Here, a subcritical pitchfork bifurcation occurs as the bifurcation parameter s decreases. The bifurcating branch recovers its stability at a fold point, and a family of stable equilibria on this branch corresponds to a family of unimodal solutions of (3.3).

Remark 3. If $(w(x), u(x))$ is an equilibrium of (3.7) with (3.8), then so is $(w(x - \pi), u(x - \pi))$. This fact implies that two branches bifurcating from a pitchfork bifurcation point cannot be distinguished in the bifurcation diagrams presented in Figs. 6 and 7, because we used the L^2-norm of the u-component as the vertical axis in the bifurcation diagrams.

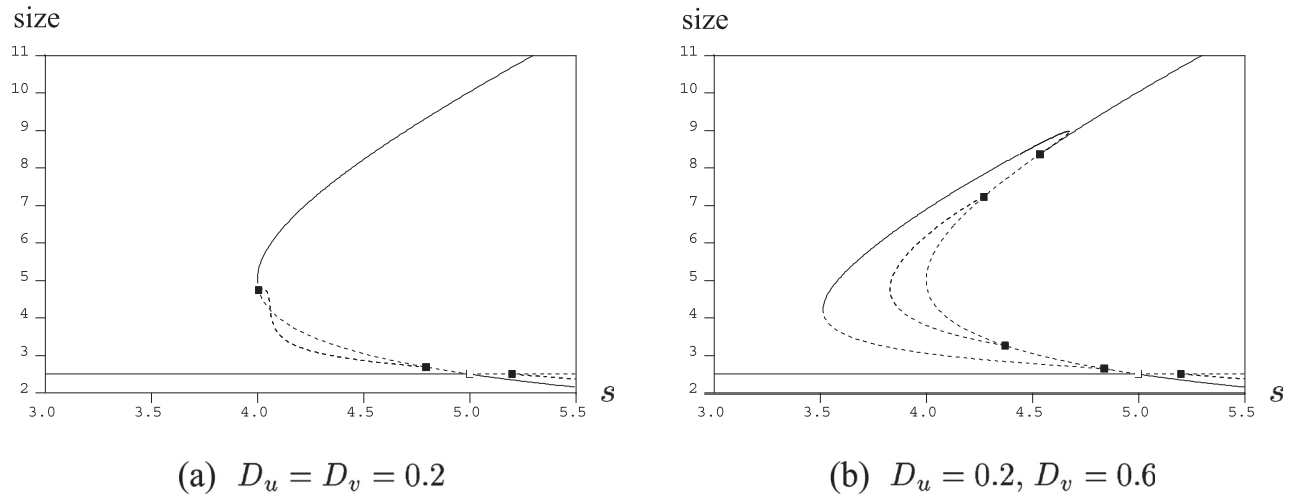

FIG. 6. The bifurcation diagrams of (3.10) with respect to s for (a) $D_u = D_v = 0.2$ and (b) $D_u = 0.2$ and $D_v = 0.6$, where s corresponds to the conserved quantity of (3.3) defined by (3.6). Other parameter values are given by $a = 4.0$, $b = 1.0$, and $N = 30$. The horizontal and vertical axes indicate s and the size (in the L^2-sense) of the u-component of solutions, respectively. The solid line indicates stable solutions, whereas the dashed line indicates unstable ones. The white and black squares indicate the transcritical and pitchfork bifurcation points, respectively. Notice that the two branches bifurcating from a pitchfork bifurcation point are piled up and are displayed in these bifurcation diagrams (see Remark 3).

By combining the bifurcation analysis for (3.10) performed using AUTO as described above with the linear stability analysis for spatially homogeneous equilibria of (3.3) and the numerical simulations for (3.3), we see that the bifurcation diagram of (3.3) with respect to s defined by (3.6) for $D_v > D_u$ contains the structure presented in Fig. 8. In fact, the numerical bifurcation analysis for (3.10) performed using AUTO can detect Γ_1, Γ_2, and Γ_4. Moreover, with the aid of the linear stability analysis for spatially homogeneous equilibria of (3.3), we find that a subcritical pitchfork bifurcation primarily occurs on Γ_1 as the bifurcation parameter s decreases, and that the branches primarily bifurcating from Γ_1 can be approximated by the Fourier modes $e^{\pm ix}$ near the subcritical bifurcation point. However, the numerical bifurcation analysis cannot guarantee the stability of Γ_1, Γ_2, and Γ_4 because (3.10) does not include the component approximated by the Fourier sine series expansion in the dynamics of (3.3) under the periodic boundary condition. Therefore, we confirm their stability using the standard linear stability analysis for spatially homogeneous equilibria or by the numerical simulations for (3.3) under the periodic boundary condition.

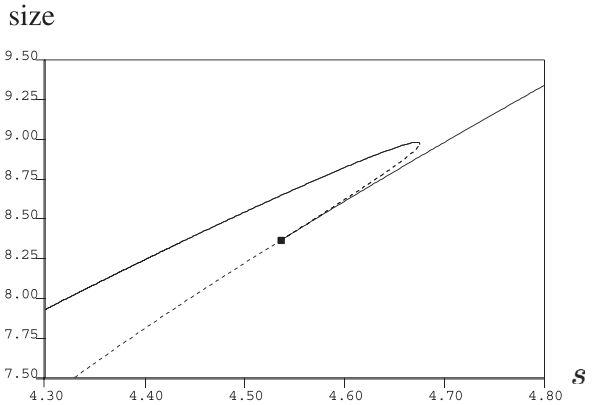

FIG. 7. A magnification of the rectangular region $[4.3, 4.8] \times [7.5, 9.5]$ in Fig. 6(b). The type of pitchfork bifurcation is subcritical as the value of s decreases.

The structure presented in Fig. 8 plays a key role in constructing a spatially nonhomogeneous limit cycle of (3.1). In the same manner as for the ODE case treated in Section II, we see that (3.1) can have a spatially nonhomogeneous limit cycle consisting of the branches Γ_1, Γ_2, and Γ_4, and the jumps from Γ_1 to Γ_4, from Γ_4 to Γ_2, and from Γ_2 to Γ_1. Here, these jumps are given by the fast dynamics (3.3), and the dynamics around Γ_1, Γ_2, and Γ_4 are given by the slow dynamics explained in Subsection III B.

Remark 4. For $f(u, v) = v - u/(u^2 + c)$ with $c > 0$, it was proved in Ref. 22 that in the bifurcation diagram of (3.3)

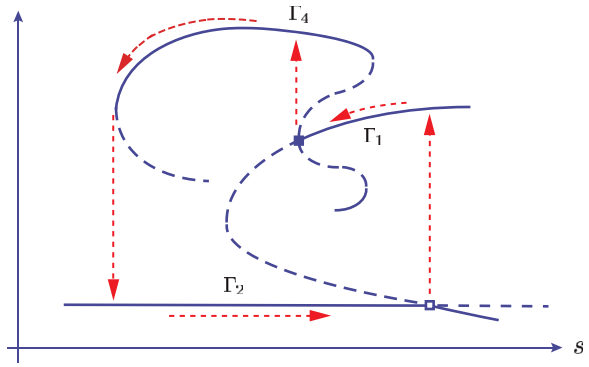

FIG. 8. A conceptual picture of the bifurcation diagram of (3.3) with respect to s. The solid line indicates stable solutions, whereas the dashed line indicates unstable ones. The white and black squares indicate the transcritical and subcritical pitchfork bifurcation points, respectively. Branches not primarily bifurcating from Γ_1 (corresponding to the unstable Fourier modes e^{ikx} ($|k| \geq 2$)) are omitted here. The dashed arrows indicate the dynamics of (3.1). Those in the vertical direction indicate the fast dynamics given by (3.3), which drives the jumps from Γ_2 to Γ_1, from Γ_1 to Γ_4, and from Γ_4 to Γ_2. The other dashed arrows indicate the slow dynamics to be considered in Subsection III B. This structure plays a key role in constructing a spatially nonhomogeneous limit cycle of (3.1).

a subcritical pitchfork bifurcation primarily occurs on a branch consisting of spatially homogeneous equilibria as s decreases.

B. Slow dynamics

We consider the dynamics of (3.1) around Γ_1, Γ_2, and Γ_4. Since these manifolds are parameterized by s, we have to extract the dynamics of s from (3.1), where s is given by (3.6). Adding the first and second equations in (3.1) and integrating over $[0, 2\pi]$, we have

$$\dot{s} = \frac{\varepsilon}{2\pi}\int_0^{2\pi} \big(g(u,v) + h(u,v)\big)dx \tag{3.11}$$

by the periodic boundary condition. This equation provides a good approximation for the dynamics around Γ_1 and Γ_2, which are equivalent to those of (2.1), as given by (2.11) and (2.12). In order to understand the dynamics around Γ_4, we numerically evaluate the value of the right hand side of (3.11) for each $(u, v) \in \Gamma_4$.

Let

$$F(s; D_v) := \frac{\varepsilon}{2\pi}\int_0^{2\pi} \big(g(u,v) + h(u,v)\big)dx,$$

where $(u, v) \in \Gamma_4$ is parameterized by s. We can obtain the graph of $F(s; D_v)$ numerically for each $D_v > D_u$ by using AUTO. For example, under the parameter values given by (2.14) and $D_u = 0.2$, the graphs of $F(s; D_v)$ for $D_v = 0.3$ and $D_v = 0.6$ are shown in Fig. 9. Consequently, we obtain the following results.

- $F(s; D_v)$ is a monotone decreasing function in s
- There exists $D_v^* > 0$ such that the following holds: (i) $F(s; D_v) < 0$ holds for any s if $D_v > D_v^*$; (ii) $F(s; D_v) = 0$ holds for some s if $D_u < D_v < D_v^*$.

We numerically confirm $D_v^* \approx 0.463$ under the parameter values given by (2.14) and $D_u = 0.2$.

From the above results, we expect that solutions of (3.1) moving along Γ_4 can reach the fold point at the left end of Γ_4 for $D_v > D_v^*$, which implies that (3.1) can have a spatially nonhomogeneous limit cycle indicated by the structure in the bifurcation diagram of (3.3) presented in Fig. 8. In contrast, they cannot reach the fold point for $D_v < D_v^*$, which implies that solutions of (3.1) converge to an equilibrium on Γ_4, i.e., a spatially nonhomogeneous limit cycle cannot be observed.

C. Numerical simulations

We numerically solve (3.1) for various values of D_v under the parameter values given by (2.14) and

$$\varepsilon = 0.01 \quad \text{and} \quad D_u = 0.2. \tag{3.12}$$

The initial value $(u_0(x), v_0(x))$ is given by a small random perturbation on the value $(2.5, 1.6) \in \Gamma_1$. Notice that the small random perturbation is an indispensable factor in the nonhomogeneous spatial pattern formation. The results presented below can also be obtained near the parameters and initial values specified above.

Our simulations are based on a standard pseudospectral method,[7,8] and the numerical scheme is presented in Appendix A. We add a small white noise to a standard scheme to prevent numerical solutions from dropping into the ODE dynamics given by (2.1) around Γ_1 and Γ_2. This small white noise can be regarded as a round-off error, and its effect on numerical results are discussed in Appendixes B and C. In simple terms, the results are summarized as follows: (i) Numerical solutions exhibit a spatially homogeneous limit cycle as presented in Fig. 10(a) for $0.2 \lesssim D_v \lesssim 0.33$, which is the same one as in Fig. 4. (ii) Numerical solutions converge to a unimodal equilibrium on Γ_4 as presented in Fig. 10(b) for $0.34 \lesssim D_v \lesssim 0.47$. (iii) Numerical solutions exhibit a spatially nonhomogeneous limit cycle as presented in Fig. 10(c) (Multimedia view) for $D_v \gtrsim 0.48$, which is indicated by Fig. 8. Notice that the deviation from the estimate $D_v^* \approx 0.463$ which distinguishes (ii) from (iii) should be considered to be within the numerical error range.

Remark 5. The transition from the case (i) to (ii) as D_v increases constitutes a delicate situation. When $D_v \approx 0.2$, no numerical solutions can leave Γ_1 within a relatively short

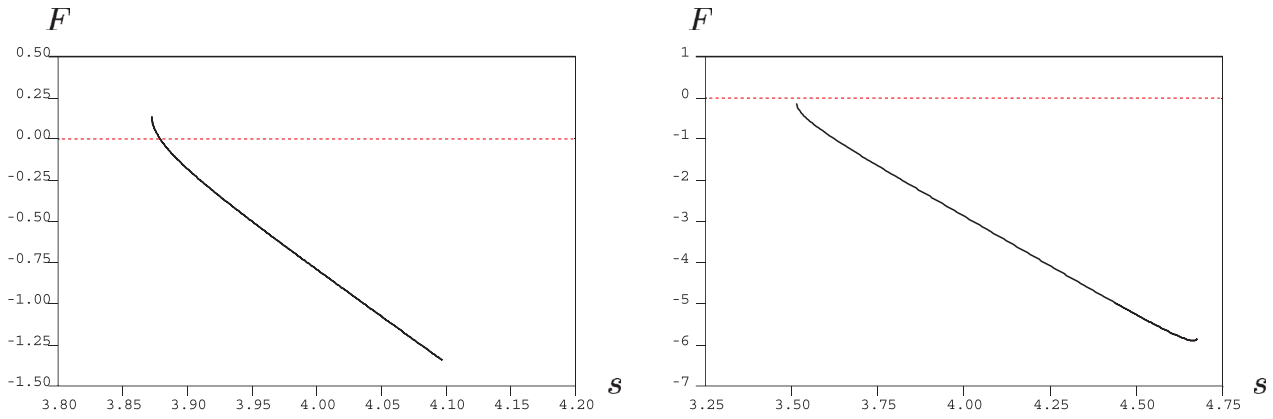

(a) $D_v = 0.3$ (b) $D_v = 0.6$

FIG. 9. The graph of $F(s; D_v)$ for (a) $D_v = 0.3$ and (b) $D_v = 0.6$. Other parameter values are given by (2.14) and $D_u = 0.2$. The horizontal and vertical axes indicate s and the value of $F(s; D_v)$, respectively.

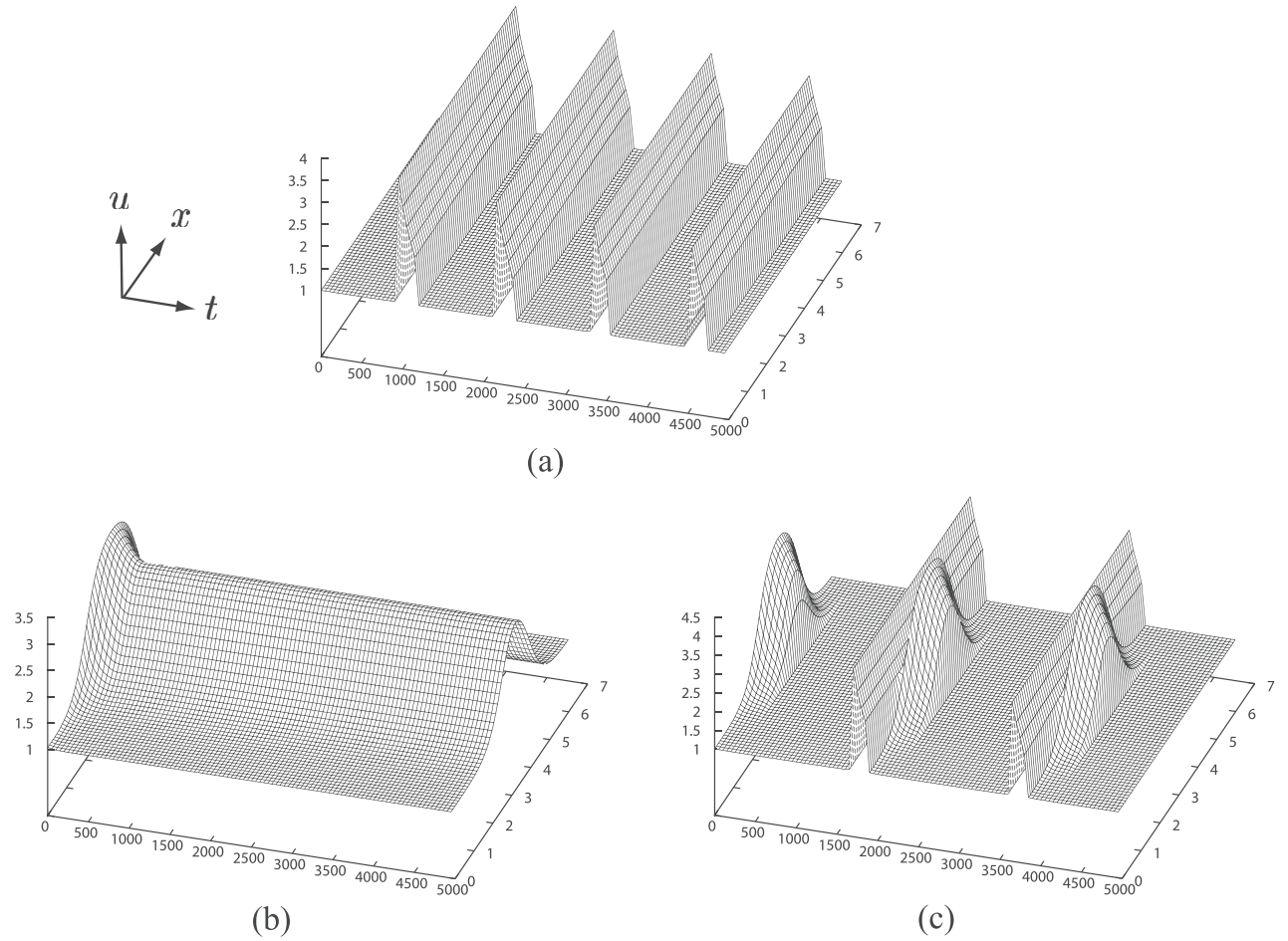

FIG. 10. The diffusion-driven destabilization of a spatially homogeneous limit cycle in (3.1) with (2.5) and (2.9); (a) $D_v = 0.3$, (b) $D_v = 0.4$, and (c) $D_v = 0.6$. Other parameter values are given by (2.14) and (3.12), and the initial value is given by $(2.5 + \varepsilon_1(x), 1.6 + \varepsilon_2(x))$, where $\varepsilon_1(x)$ and $\varepsilon_2(x)$ are independent uniform pseudorandom numbers in $[-0.005, 0.005)$ for each $x \in [0, 2\pi]$. The values of $u(x, t)$ on $0 \le x \le 2\pi$ and $0 \le t \le 5000$ are represented by a 3D graph. The profile of $v(x, t)$ is omitted here because the amplitude and spatial variation of $v(x, t)$ for each t are relatively small compared to those of $u(x, t)$. As the value of D_v increases, the spatially homogeneous limit cycle becomes unstable, and eventually changes to a stable spatially nonhomogeneous limit cycle. An animation shows the behavior of the spatially nonhomogeneous limit cycle for $0 \le t \le 5000$. We recommend that the readers watch the animated movie file of how the spatial pattern is changing; the green and yellow curves represent u and v, respectively. (Multimedia view) [URL: http://dx.doi.org/10.1063/1.4978924.1]

time because the effect of the diffusion-driven destabilization is weak. Consequently, they can move along Γ_1 and reach the fold point at the left end of Γ_1. This effect becomes stronger as D_v increases. When $0.33 \lesssim D_v \lesssim 0.34$, numerical solutions either can jump from Γ_1 to Γ_4 near the subcritical pitchfork bifurcation point on Γ_1, or can move along Γ_1. For example, we may observe that a numerical solution approaching the subcritical pitchfork bifurcation point for the first time jumps from Γ_1 to Γ_4, but the numerical solution approaching for the second time can move along Γ_1. As D_v increases further, all numerical solutions jump from Γ_1 to Γ_4 near the subcritical pitchfork bifurcation point on Γ_1.

Remark 6. The positions of the peaks of unimodal patterns that repeatedly appear at a certain period vary in the case (iii). This reflects the fact that the definition of the stability of an equilibrium or periodic orbit of PDEs under the periodic boundary condition allows the freedom of translation in the spatial direction.

Remark 7. When the amplitude of a white noise incorporated into our numerical scheme is too small, it occurs that numerical solutions drop into the ODE dynamics given by (2.1) even if D_v/D_u is relatively large. In fact, a numerical solution approaching the subcritical pitchfork bifurcation point for the first time can jump from Γ_1 to Γ_4 because we add a small random perturbation to its initial value on Γ_1. However, after passing through Γ_2, the numerical solution returning to the subcritical pitchfork bifurcation point for the second time can pass through the subcritical pitchfork bifurcation point on Γ_1, and can continue to move along Γ_1. Thereafter, the numerical solution continues to move along a closed orbit, as given by Fig. 4. In this case, the numerical solutions drop into the ODE dynamics around Γ_2 that attracts solutions strongly.

Remark 8. We consider (3.1) with small diffusion coefficients. This is equivalent to the case of large system size by rescaling spatial variables. Fig. 11 (Multimedia view) shows an alternating repetition of complex dynamics and spatially (almost) homogeneous oscillations for $D_u = 0.02$ and $D_v = 0.24$. This corresponds to a spatially nonhomogeneous limit cycle as presented in Fig. 10(c), which shows an alternating repetition of simple unimodal patterns and spatially (almost) homogeneous oscillations. In this complex dynamics, there appear spatial patterns consisting of spikes. The number of spikes decreases, as observed in the dynamics of

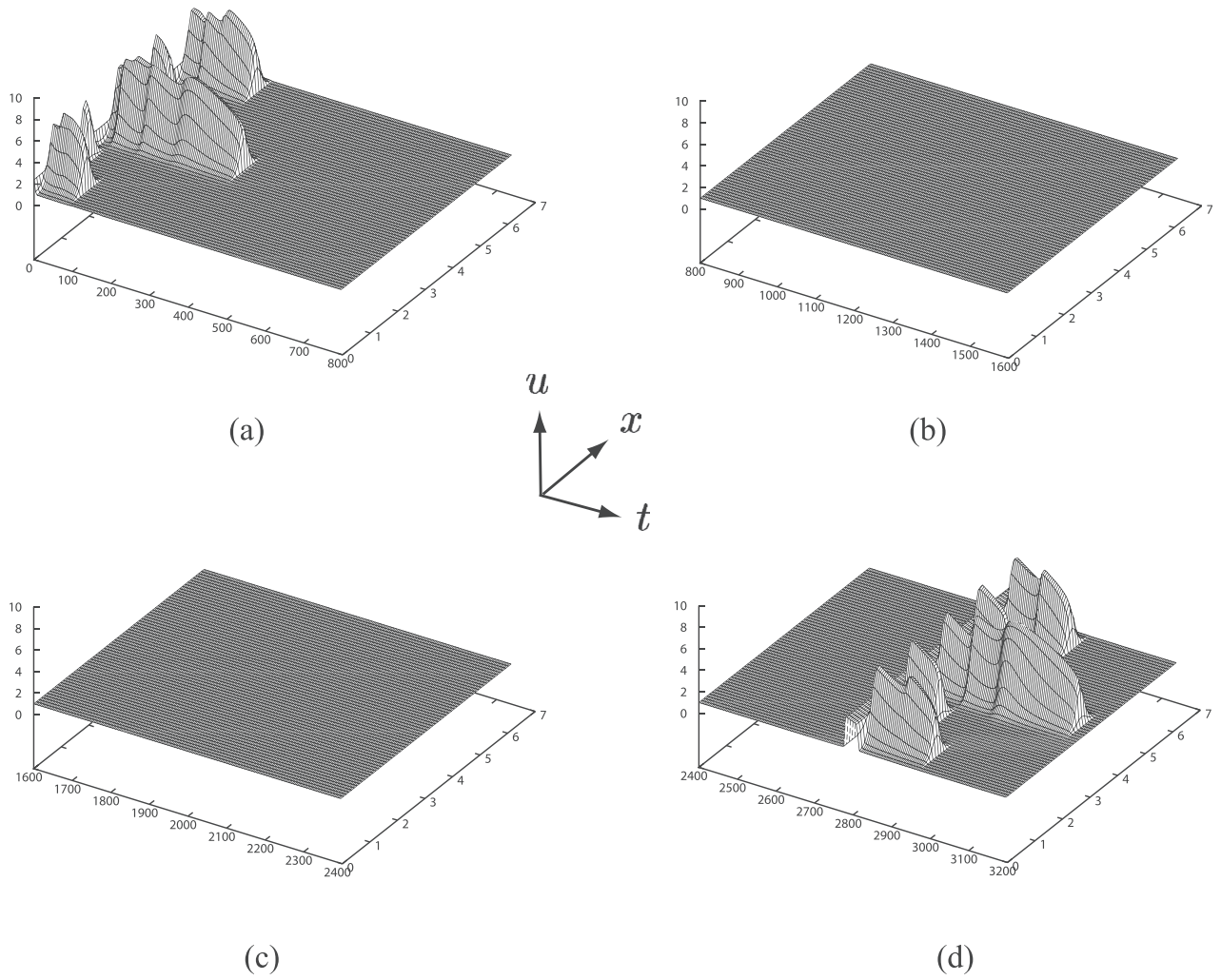

FIG. 11. An alternating repetition of complex dynamics and spatially (almost) homogeneous oscillations in the dynamics of (3.1) with (2.5) and (2.9) for $D_u = 0.02$ and $D_v = 0.24$; (a) $0 \le t \le 800$, (b) $800 \le t \le 1600$, (c) $1600 \le t \le 2400$, and (d) $2400 \le t \le 3200$. Other parameter values are given by (2.14) and $\varepsilon = 0.01$, and the initial value is given by $(2.5 + \varepsilon_1(x), 1.6 + \varepsilon_2(x))$, where $\varepsilon_1(x)$ and $\varepsilon_2(x)$ are independent uniform pseudorandom numbers in $[-0.005, 0.005)$ for each $x \in [0, 2\pi]$. The values of $u(x, t)$ on $0 \le x \le 2\pi$ and $0 \le t \le 3200$ are represented by a 3D graph. The profile of $v(x, t)$ is omitted here because the amplitude and spatial variation of $v(x, t)$ for each t are relatively small compared to those of $u(x, t)$. In this complex dynamics, there appear spatial patterns consisting of spikes, and the number of spikes decreases. An animation shows the behavior of the alternating repetition for $0 \le t \le 6400$. We recommend that the readers watch the animated movie file of how the spatial pattern is changing; the green and yellow curves represent u and v, respectively. (Multimedia view) [URL: http://dx.doi.org/10.1063/1.4978924.2]

(3.3). Although (3.5) suggests that the number of spikes generated at the first stage of the complex dynamics increases as the values of D_u and D_v decrease, we cannot predict this number of spikes because the spike-generating dynamics takes place far from the local dynamics indicated by the linear stability analysis around equilibria. We note that such an alternating repetition as presented in Fig. 11 cannot be treated by a rigorous mathematical analysis.

Thus, we have presented a simple two-component reaction-diffusion model in which a spatially homogeneous limit cycle becomes unstable and changes to a spatially nonhomogeneous stable limit cycle for appropriate diffusion coefficients. This constitutes the diffusion-driven destabilization of a spatially homogeneous limit cycle, which is analogous to the well-known case of an equilibrium. Our method of constructing a spatially nonhomogeneous limit cycle of a reaction-diffusion system would be valid from an analogy of the theory of finite dimensional slow-fast systems.

IV. CONCLUDING REMARKS

In this paper, we have demonstrated that a spatially homogeneous limit cycle becomes unstable and changes to a spatially nonhomogeneous stable limit cycle for appropriate diffusion coefficients in a two-component reaction-diffusion system that is defined on a finite interval under the periodic boundary condition. To the best of our knowledge, this is a clear new example of the diffusion-driven destabilization (Turing instability) of limit cycles. In fact, previous studies considered a limit cycle with small amplitude near a Hopf bifurcation point or a limit cycle of the complex Ginzburg-Landau equation, whose specific nonlinear terms allow us to obtain a concrete expression of the limit cycle. Moreover, our numerical bifurcation analysis by using AUTO indicates the infinite dimensional dynamical picture of our reaction-diffusion model, and supports the results of numerical simulations.

Our approach is based on a reaction-diffusion system with mass conservation and its perturbed system. For each

set of diffusion coefficients in the unperturbed reaction-diffusion system, the total mass is conserved. Varying the total mass in the unperturbed system, we obtain a bifurcation diagram regarding the total mass as a bifurcation parameter. Upon adding perturbations, the total mass is no longer conserved. Therefore, on the stable branches in the bifurcation diagram, the perturbations induce slow dynamics. Combining the slow dynamics induced on the total mass with the fast dynamics generated by the original unperturbed systems, we obtain a spatially nonhomogeneous limit cycle in the perturbed reaction-diffusion system for appropriate diffusion coefficients. Thus, we can understand the diffusion-driven destabilization of a spatially homogeneous limit cycle as the creation of the spatially nonhomogeneous limit cycle due to the appropriate transitions of slow-fast dynamic bifurcation diagrams as the diffusion coefficients vary.

The critical factor in our approach is the choice of the nonlinear term of a reaction-diffusion system with mass conservation, which determines the fast dynamics generating a simple localized unimodal pattern. For this nonlinear term, various functions have been proposed, see Refs. 10, 17, 18, 20, and 25. According to the mathematical analysis presented in Refs. 11, 16, 21, and 22, we expect that a certain large class of functions induces such dynamics in reaction-diffusion systems with mass conservation. Therefore, it is likely to observe a spatially nonhomogeneous limit cycle induced by the diffusion-driven destabilization in a reaction-diffusion system that is obtained by adding diffusion terms to a slow-fast ODE system, where the sum of components of the fast ODE system is conserved. Thus, our method, which was presented in this study through a concrete example, is useful in obtaining a spatially nonhomogeneous limit cycle induced by the diffusion-driven destabilization.

Recently, Ref. 3 proposed a condition for the instability of limit cycles in diffusively coupled oscillators, which can be regarded as a spatial discretization of reaction-diffusion systems. However, in contrast to the case of equilibria, there are not enough studies on the diffusion-driven destabilization of limit cycles. This reflects the fact that the existence and stability of limit cycles in reaction-diffusion systems cannot be mathematically verified without specific assumptions. In this study, we assume the mass conservation property of an unperturbed reaction-diffusion system and consider the perturbed system from the viewpoint of the theory of slow-fast systems. At the present time, we do not know how to study the diffusion-driven destabilization of a spatially homogeneous limit cycle with large amplitude in general reaction-diffusion systems.

ACKNOWLEDGMENTS

The authors express their sincere gratitude to Professor Kunimochi Sakamoto and Dr. Sungrim Seirin Lee for their useful advice and comments. Moreover, the authors would like to express their appreciation to the referees for their useful suggestions and comments which have improved the original manuscript. The first and second authors were supported in part by the JSPS Grant-in-Aid for Scientific Research (C) No. 16K05273 and for Young Scientists (B) No. 26800084, respectively.

APPENDIX A: NUMERICAL SCHEME

By applying the Fourier transformation, a reaction-diffusion system in the real space

$$u_t = Du_{xx} + f(u) \tag{A1}$$

can be converted to an ODE system in the Fourier space

$$\frac{d\widehat{u}_k}{dt} = -Dk^2\widehat{u}_k + f_k(\widehat{u}), \tag{A2}$$

where k denotes the wavenumber, and

$$f_k(\widehat{u}) = (\widehat{f(u)})_k = (\mathcal{F}(f(\mathcal{F}^{-1}\widehat{u})))_k$$

with the Fourier transformation $\mathcal{F}$ and its inverse $\mathcal{F}^{-1}$. In simple terms, the pseudospectral method for numerically solving (A1) on $(-L/2, L/2)$ under the periodic boundary condition is a numerical scheme to solve (A2) by using the Runge–Kutta method under the condition that the amplitudes of high frequency Fourier modes $e^{2\pi ikx/L}$ vanish; $\widehat{u}_k = 0\,(k \in \mathbf{Z},\ |k| \geq N/2)$, where $N = 2^m\,(m \in \mathbf{N})$ is the total number of Fourier modes in the numerical computation (finite dimensional approximation) with the aid of FFT.

Let $v_k = \widehat{u}_k \exp(-Dk^2t)$. Then, we have

$$\frac{dv_k}{dt} = f_k(\widehat{u})\exp(Dk^2t) := G_k(v,t). \tag{A3}$$

By applying the fourth order Runge–Kutta scheme to (A3), we have

$$\begin{aligned}
&v_k(t+\Delta t) = v_k(t) + (h_1 + 2h_2 + 2h_3 + h_4)\Delta t/6,\\
&h_1 = G_k(v,t) = f_k(\widehat{u})\exp(Dk^2t),\\
&\widehat{u}_1' = \{\widehat{u}_k(t) + h_1\exp(-Dk^2t)\Delta t/2\}\exp(-Dk^2\Delta t/2),\\
&h_2 = G_k(v + h_1\Delta t/2,\ t + \Delta t/2) = f_k(\widehat{u}_1')\exp\left(Dk^2(t+\Delta t/2)\right),\\
&\widehat{u}_2' = \{\widehat{u}_k(t) + h_2\exp(-Dk^2t)\Delta t/2\}\exp(-Dk^2\Delta t/2),\\
&h_3 = G_k(v + h_2\Delta t/2,\ t + \Delta t/2) = f_k(\widehat{u}_2')\exp\left(Dk^2(t+\Delta t/2)\right),\\
&\widehat{u}_3' = \{\widehat{u}_k(t) + h_3\exp(-Dk^2t)\Delta t\}\exp(-Dk^2\Delta t),\\
&h_4 = G_k(v + h_3\Delta t,\ t + \Delta t) = f_k(\widehat{u}_3')\exp\left(Dk^2(t+\Delta t)\right).
\end{aligned}$$

Thus, we obtain the following numerical scheme for (A2):

$$\begin{aligned}
\widehat{u}_k(t+\Delta t) = {}& \widehat{u}_k(t)\exp(-Dk^2\Delta t)\\
&+\{h_1'\exp(-Dk^2\Delta t) + 2(h_2' + h_3')\\
&\times\exp(-Dk^2\Delta t/2) + h_4'\}\Delta t/6
\end{aligned}$$

where

$$h_1' = f_k(\widehat{u}),\ h_2' = f_k(\widehat{u}_1'),\ h_3' = f_k(\widehat{u}_2'),\ h_4' = f_k(\widehat{u}_3').$$

Although numerical schemes to solve PDEs by using the pseudospectral method are rather more involved than standard finite difference schemes, they can provide precise numerical results even if the PDEs satisfy (infinitely many) conservation laws such as the KdV equation.[7,8]

In our simulations, we use the following numerical scheme:

$$\begin{aligned}\widehat{u}_k(t+\Delta t) = \widehat{u}_k(t)\exp(-Dk^2\Delta t) \\ +\{h_1'\exp(-Dk^2\Delta t) + 2(h_2'+h_3') \\ \times \exp(-Dk^2\Delta t/2) + h_4'\}\Delta t/6 + \mu_k(t),\end{aligned}$$

where $\mu_k(t)$ is a small white noise that prevents numerical solutions from dropping into the ODE dynamics without the diffusion terms.

APPENDIX B: THE EFFECT OF A SMALL WHITE NOISE

Considering a small white noise incorporated into a numerical scheme as a round-off error, the fourth order Runge–Kutta scheme for numerically solving an ODE system $du/dt = G(u, t)$ is given by

$$v_{n+1} = v_n + (h_1 + 2h_2 + 2h_3 + h_4)\Delta t/6 + \mu_n,$$

where

$$\begin{aligned}&h_1 = G(v_n, t), \quad h_2 = G(v_n + h_1\Delta t/2,\ t + \Delta t/2),\\ &h_3 = G(v_n + h_2\Delta t/2,\ t + \Delta t/2),\\ &h_4 = G(v_n + h_3\Delta t,\ t + \Delta t)\end{aligned}$$

and μ_n denotes a small white noise. Under the assumption that $v_0 = u(0)$, a standard argument shows (e.g., Ref. 2) that the error estimation

$$|u(n\Delta t) - v_n| \le CN((\Delta t)^5 + \mu)$$

holds, where $\mu = \max|\mu_n|$, $N = T/(\Delta t)$ denotes the total number of iterations, and C denotes a constant which is independent of Δt, μ, and N. It should be noted that the above error estimation is given by the truncation error $CN(\Delta t)^5 (= CT(\Delta t)^4)$ if $|\mu| = 0$. From the above estimation, we can conclude that if $|\mu| \ll (\Delta t)^5$, then the white noise does not affect the numerical results obtained by the fourth order Runge–Kutta scheme. In our numerical simulations, we take $\Delta t = 10^{-2}$ and $\mu = 10^{-11}$ or 10^{-12}. Hence, our numerical results are valid. In other words, we need not apply an error estimation based on the theory of SDEs, which is useful if the randomness of a white noise significantly affects the results of a numerical simulation.[9]

When $\mu = 10^{-m} (m \ge 13)$, it occurs that our numerical solutions drop into the ODE dynamics, as mentioned in Remark 7. In contrast, when $\mu = 10^{-m} (5 \le m \le 10)$, we can also obtain the same numerical results even though the amplitude of the white noise is not smaller than the truncation error. In Appendix C, we provide a reason why relatively large white noises do not affect our numerical results.

APPENDIX C: NON-DIVERGENCE OF THE ACCUMULATION OF ERRORS IN NUMERICAL COMPUTATIONS

In general, a PDE system is formulated as an evolution equation on a Banach space. For example, our reaction-diffusion system (3.1) is formulated as an evolution equation

$$\frac{dy}{dt} = Ay + F(y) \tag{C1}$$

on $L^2(0, 2\pi) \times L^2(0, 2\pi)$ equipped with the usual L^2-norm, where $y = (u, v)$, $A = \mathrm{diag}(D_u\partial_x^2, D_v\partial_x^2)$ and $F(y) = (f(u, v) + \varepsilon g(u, v), -f(u, v) + \varepsilon h(u, v))$. Let z be an approximate solution of (C1) such that if $z(t_0) = y(t_0)$ holds for some $t_0 \ge 0$, then

$$\sup_{t_0 \le t \le t_0 + T} ||z(t) - y(t)|| < \delta \tag{C2}$$

holds for some $T > 0$, where T depends on only $\delta > 0$. We consider that z is a numerical solution of (3.1), which is obtained by using our numerical scheme. We note that δ gives an upper bound on the accumulation of all errors on the time interval $[t_0, t_0 + T]$. Therefore, the accumulation of the effects of white noises in our numerical simulation is included in δ.

Theorem C. 1. Suppose that

$$||y_1(t) - y_2(t)|| \le Ce^{-\alpha(t-t_0)}||y_1(t_0) - y_2(t_0)|| \tag{C3}$$

holds, where y_1 and y_2 are solutions of (C1) and $L := Ce^{-\alpha T} < 1$. Then,

$$\sup_{0 \le t < \infty} ||z(t) - y(t)|| < \frac{\delta}{1 - L}$$

holds if $z(0) = y(0)$.

Proof. By $\tilde{y}_s$, we denote a solution of (C1) satisfying $\tilde{y}_s(s) = z(s)$. Let us take $\tau > T$ arbitrarily. Noting that

$$\tau = mT + r, \quad m \in \mathbf{N}, \quad 0 \le r < T,$$

we have

$$\begin{aligned}||z(\tau) - y(\tau)|| &\le ||z(\tau) - \tilde{y}_{\tau-T}(\tau)|| \\ &\quad + \sum_{k=1}^{m-1} ||\tilde{y}_{\tau-kT}(\tau) - \tilde{y}_{\tau-(k+1)T}(\tau)|| + ||\tilde{y}_{\tau-mT}(\tau) - y(\tau)|| \\ &= ||z(\tau) - \tilde{y}_{\tau-T}(\tau)|| + \sum_{k=1}^{m-1} ||\tilde{y}_{\tau-kT}(\tau) - \tilde{y}_{\tau-(k+1)T}(\tau)|| \\ &\quad + ||\tilde{y}_r(\tau) - y(\tau)||.\end{aligned}$$

Since $\tilde{y}_{\tau-T}$ is a solution of (C1) satisfying $\tilde{y}_{\tau-T}(\tau - T) = z(\tau - T)$, it follows from (C2) that

$$||z(\tau) - \tilde{y}_{\tau-T}(\tau)|| < \delta.$$

Moreover, noting (C3), we have

$$\begin{aligned}||\tilde{y}_{\tau-T}(\tau) - \tilde{y}_{\tau-2T}(\tau)|| &\le L||\tilde{y}_{\tau-T}(\tau - T) - \tilde{y}_{\tau-2T}(\tau - T)|| \\ &= L||z(\tau - T) - \tilde{y}_{\tau-2T}(\tau - T)|| < L\delta\end{aligned}$$

by virtue of (C2) because $\tilde{y}_{\tau-2T}$ is a solution of (C1) satisfying $\tilde{y}_{\tau-2T}(\tau - 2T) = z(\tau - 2T)$. Similarly, we have

$$||\tilde{y}_{\tau-kT}(\tau) - \tilde{y}_{\tau-(k+1)T}(\tau)|| < L^k\delta \quad (2 \le k \le m - 1)$$

and

$$||\tilde{y}_r(\tau) - y(\tau)|| < L^m\delta.$$

Therefore, we have

$$||z(\tau) - y(\tau)|| \le \delta + L\delta + \cdots + L^m\delta = \frac{\delta(1 - L^{m+1})}{1 - L} < \frac{\delta}{1 - L}.$$

Thus, we have

$$\sup_{0\le t<\infty} ||z(t) - y(t)|| = \max\left(\sup_{0\le t\le T} ||z(t) - y(t)||, \sup_{t\ge T} ||z(t) - y(t)|| \right) = \max\left(\delta, \frac{\delta}{1 - L}\right) = \frac{\delta}{1 - L}. \quad \square$$

The above argument is an improved version of the proof of Ref. 27, Theorem 5.5.1, which assumed the solvability of evolution equations (ODEs) back in time. This is not necessarily true for PDEs. As seen in Ref. 27, Section 5, we can assume that (C3) holds near a stable object (e.g., equilibrium or periodic orbit) that exponentially attracts solutions around it. Therefore, Theorem C.1 gives a mathematical justification for our naive intuition that white noises and truncation errors can be dissipated by an intrinsic stabilization effect of evolution equations around stable objects with exponential attractivity. Thus, we can conclude that the effect of white noise in our scheme does not accumulate during numerical computations.

[1]N. Berglund and B. Gentz, *Noise-Induced Phenomena in Slow-Fast Dynamical Systems* (Springer-Verlag, New York, 2006).
[2]J. C. Butcher, *Numerical Methods for Ordinary Differential Equations* (John Wiley & Sons, 1987).
[3]J. D. Challenger, R. Burioni, and D. Fanelli, "Turing-like instabilities from a limit cycle," Phys. Rev. E **92**, 022818 (2015).
[4]M. C. Cross and P. C. Hohenberg, Rev. Mod. Phys. **65**, 851–1112 (1993).
[5]E. J. Doedel, A. R. Champneys, T. F. Fairgrieve, Y. A. Kuznetsov, B. E. Oldeman, R. C. Paffenroth, B. Sandstede, and X. Wang, AUTO 2000: Continuation and bifurcation software for ordinary differential equations (with HomCont), 2000.
[6]S.-I. Ei, H. Izuhara, and M. Mimura, "Infinite dimensional relaxation oscillation in aggregation-growth systems," DCDS Ser. B **17**, 1859–1887 (2012).
[7]B. Fornberg, *A Practical Guide to Pseudospectral Methods* (Cambridge University Press, 1995).
[8]D. Gottlieb and S. A. Orszag, *Numerical Analysis of Spectral Methods: Theory and Applications* (SIAM-CBMS, 1977).
[9]H. S. Greenside and E. Helfand, "Numerical integration of stochastic differential equations II," Bell Syst. Tech. J. **60**, 1927–1940 (1981).
[10]S. Ishihara, M. Otsuji, and A. Mochizuki, "Transient and steady state of mass-conserved reaction-diffusion systems," Phys. Rev. E **75**, 015203 (2007).
[11]S. Jimbo and Y. Morita, "Lyapunov function and spectrum comparison for a reaction-diffusion system with mass conservation," J. Differ. Equations **255**, 1657–1683 (2013).
[12]J. Keener and J. Sneyd, *Mathematical Physiology I*, 2nd ed. (Springer-Verlag, New York, 2008).
[13]Y. Kuramoto, "Diffusion-induced chaos in reaction systems," Prog. Theor. Phys. Suppl. **64**, 346–367 (1978).
[14]Y. Kuramoto, *Chemical Oscillations, Waves, and Turbulence* (Springer-Verlag, Berlin Heidelberg, 1984).
[15]M. Kuwamura and Y. Morita, "Perturbations and dynamics of reaction-diffusion systems with mass conservation," Phys. Rev. E **92**, 012908 (2015).
[16]E. Latos and T. Suzuki, "Global dynamics of a reaction-diffusion system with mass conservation," J. Math. Anal. Appl. **411**, 107–118 (2014).
[17]S. Seirin Lee, "Positioning of polarity formation by extracellular signaling during asymmetric cell division," J. Theor. Biol. **400**, 52–64 (2016).
[18]S. Seirin Lee and T. Shibata, "Self-organization and advective transport in the cell polarity formation for asymmetric cell division," J. Theor. Biol. **382**, 1–14 (2015).
[19]K. Maginu, "Stability of spatially homogeneous periodic solutions of reaction-diffusion equations," J. Differ. Equations **31**, 130–138 (1979).
[20]Y. Mori, A. Jilkine, and L. Edelstein-Keshet, "Wave-Pinning and cell polarity from a bistable reaction-diffusion system," Biophys. J. **94**, 3684–3697 (2008).
[21]Y. Morita, "Spectrum comparison for a conserved reaction-diffusion system with a variational property," J. Appl. Anal. Comput. **2**, 57–71 (2012).
[22]Y. Morita and T. Ogawa, "Stability and bifurcation of nonconstant solutions to a reaction-diffusion system with conservation of mass," Nonlinearity **23**, 1387–1411 (2010).
[23]J. D. Murray, *Mathematical Biology*, 2nd ed. (Springer-Verlag, New York, 1989).
[24]A. Okubo, *Diffusion and Ecological Problems: Mathematical Models* (Springer-Verlag, New York, 1980).
[25]M. Otsuji, S. Ishihara, C. Co, K. Kaibuchi, A. Mochizuki, and S. Kuroda, "A mass conserved reaction-diffusion system captures properties of cell polarity," PLoS Comput. Biol. **3**, e108 (2007).
[26]M. R. Ricard and S. Mischler, "Turing instabilities at Hopf Bifurcation," J. Nonlinear Sci. **19**, 467–496 (2009).
[27]J. A. Sanders, F. Verhulst, and J. Murdock, *Averaging Methods in Nonlinear Dynamical Systems*, 2nd ed. (Springer-Verlag, New York, 2007).
[28]S. H. Strogatz, *Nonlinear Dynamics and Chaos* (Westview Press, 2000).
[29]A. M. Turing, "The chemical basis of morphogenesis," Philos. R. Soc. B **237**, 37–72 (1952).
[30]M. J. Ward, "Asymptotic methods for reaction-diffusion systems: Past and present," Bull. Math. Biol. **68**, 1151–1167 (2006).